A step forward in sustainable pesticide production from *Amphidinium carterae* biomass via photobioreactor cultivation with urea as a nitrogen source

A. Molina-Miras[a,c], A.C. Abreu[b,c], L. López Rosales[a,c], M.C. Cerón-García[a,c], A. Sánchez-Mirón[a,c], I. Fernández*[b,c], F. García-Camacho*[a,c]

[a] Department of Chemical Engineering, University of Almería, 04120 Almería, Spain

[b] Department of Chemistry and Physics, University of Almería, 04120 Almería, Spain

[c] Research Center CIAIMBITAL, University of Almería, 04120 Almería, Spain

*Corresponding author: fgarcia@ual.es

Address: Department of Chemical Engineering, University of Almería, Carretera Sacramento s/n. 04120, Almería (Spain)

Telephone number: +34 950015303

Fax: +34 950 015484

*Corresponding author: ifernan@ual.es

Address: Department of Chemistry and Physics, University of Almería. Carretera Sacramento s/n. E04120, Almería, Spain.

Telephone number: +34 950214465

Graphical Abstract (for review)

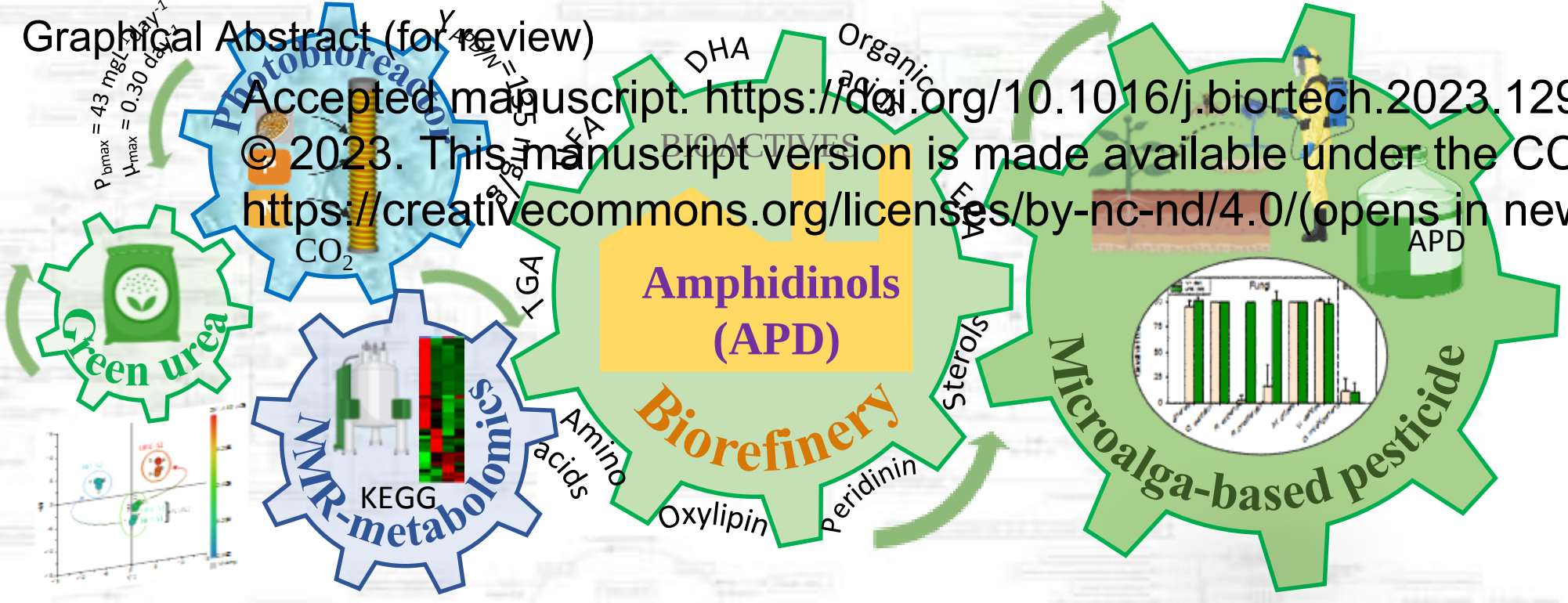

Abstract

This study addressed the problem of replacing nitrate and ammonium with urea as a greener nitrogen source in the mass cultivation of the microalga *Amphidinium carterae* for the development of amphidinol-based phytosanitary products. To solve this problem, an NMR-assisted investigation evaluated the effect of nitrogen sources on growth and metabolic profiles in photobioreactors. Urea-fed cultures exhibited growth kinetics comparable to nitrate-fed cultures (μ_{max} = 0.30 day^{-1}, P_{bmax} = 43 $mgL^{-1}day^{-1}$). Urea-fed cultures had protein, lipid, and carbohydrate contents of 39.5%, 14.5%, and 42.4%, respectively, while nitrate-fed cultures had 27.9 %, 17.5% and 48.1%, respectively. Metabolomics revealed nitrogen source-dependent metabotypes and a correlation between amphidinols and polyunsaturated fatty acids. The amphidinol-to-nitrogen yield coefficient in urea-fed cultures (135 mg/g) was approximately 2.5 times higher than in nitrate-fed cultures. The potent antiphytopathogenic activity exhibited by extracts from urea-fed cultures underscores the potential of urea as a sustainable nitrogen source in microalgae-based biorefineries.

Keywords: Microalgae; dinoflagellate; metabolomics, amphidinol; NMR

1. Introduction

Microalgae refineries are emerging as a means for cost-effectively and sustainably producing valuable products such as omega-3 fatty acids, carotenoids, proteins, or biopolymers with wide-ranging applications in human health, nutrition, agriculture, and pharmaceuticals (Park et al., 2022). Therefore, the use of sustainable nutrients in microalgal culture media is paramount to ensure a circular bioeconomy of such refineries. Nitrogen, usually in the form of ammonium, nitrate and urea, is the main macronutrient used in microalgal culture media (Su, 2021). However, all three account for most of the planet's global reactive nitrogen (Spiller et al., 2022), whose increasing production has far-reaching implications for global ecosystems. Using reactive nitrogen recovery methods to reduce environmental impacts while providing economic benefits is the preferred paradigm (Spiller et al., 2022). Microalgae-based wastewater

treatments offer an alternative to classical treatments for reactive nitrogen recovery (Urbańczyk et al., 2016; Li et al., 2019) and are part of the circular economy concept.

Unfortunately, since the ammonium toxicity thresholds for microalgae are relatively low compared to nitrate and urea, few of the known microalgae can withstand the ammonium concentrations present in most wastewaters studied. Therefore, the treatment of clean-in place wastewater (CIP) using microalgae to upcycle nutrients and produce value-added byproducts, as already reported (Su and Jacobsen, 2021), is an option limited to highly ammonium-tolerant microalgae. Additionally, the cultivation of microalgae in wastewater is questioned or prohibited for many applications where microalgae biomass is used as raw material to obtain products for human use. The alternative is the use of chemically defined culture media, for which the choice of nitrogen source is critical at industrial scale because it accounts for more than 60% by dry weight of photoautotrophically obtained microalgal biomass (excluding the contribution of C, O and H; elements incorporated by the cells from the CO_2 provided and water). In this scenario, nitrate is typically the preferred choice as the primary nitrogen source. However, it has important disadvantages compared to urea. Urea is the preferred nitrogen source for many microalgal species (Kumar and Bera, 2020). Although chemical synthesis processes are the main industrial routes for the commercial production of nitrate and urea, nitrate is also sourced from mineral deposits. However, unlike nitrate, the potential recovery of urea through various green pathways is gaining considerable momentum (Milani et al., 2022). In this sense, the production of ammonia feedstock in a 'green' way and the use of carbon-neutral CO2 sources are crucial for considering urea synthesis as a 'green' technology (Milani et al., 2022). The recent use of green hydrogen from alkaline water electrolysis demonstrates the potential feasibility of renewable urea synthesis from a technical, economic and environmental perspective (Kim et al., 2023). Accessible sources of carbon-neutral CO2, such as biomass, renewable methane and direct air carbon capture, further support sustainable urea production. Although achieving complete decarbonisation and sustainability in urea production may still be a challenge, ongoing efforts in government regulations, energy management systems and technological advancements are bringing us closer to this goal (Milani et al., 2022).

Despite urea, currently the predominant nitrogen fertiliser in agriculture, is projected to maintain its position as the primary choice for years to come (Statista, 2022), it remains a scarcely explored nitrogen source for microalgae cultivation. If microalgae of commercial interest are high-urea tolerant, urea would favour the formulation of sustainable low-cost media, boosting the development of biobased products from microalgae such as biostimulants and pesticides, which have a huge relevance in the current agricultural industry due to the increased demand for healthy and safe food (Behera et al., 2021; Renuka et al., 2018). Future and ongoing research is focused on refining these algal compounds, assessing their environmental impact, and exploring their broader applications in sustainable agriculture (Behera et al., 2021; Renuka et al., 2018). Consistent with this, the marine microalga *Amphidinium carterae* has shown great potential as a valuable resource for the development of phytosanitary products with antifungal activity under a biorefinery approach , amphidinols (APD) being their secondary metabolites that are primarly responsible for the bioactivity (Thomas and Thiebeauld, 2022; Navarro López et al., 2023; Barone et al., 2021; Mart et al., 2019). *A. carterae* is a candidate strain for the development of large-scale biorefinery because it is capable of synthesising other bioproducts of interest, such as the polyunsaturated fatty acids (PUFA) eicosapentaenoic acid (EPA), and docosahexaenoic acid (DHA), and carotenoids, which can be commercially extracted using well-established technologies for industrial bioprocesses (López-Rodríguez et al., 2021; Molina-Miras et al., 2018a).

The provision of these compounds derived from *A. carterae* seems to be guaranteed since successful cultivation of this microalga has been achieved at pilot scale in bubble column and raceway photobioreactors (PBR) (Molina-Miras et al., 2020b; Morales-Amador et al., 2021). Additionally, metabolic changes have been successfully monitored with the help of nuclear magnetic resonance (NMR) spectroscopy when culture conditions were varied in a raceway photobioreactor with nitrate as a nitrogen source (Abreu et al., 2019). In fact, NMR metabolomics has positively impacted microalgae biomolecule production due to its robustness, reproducibility, and ability to identify and quantify many of these added-value components without the need for internal standards (López-Rodríguez et al., 2021).

In this work, for the first time, an NMR-aided proof-of-concept study was conducted to evaluate the impact of urea as a green nitrogen source, compared to nitrate and ammonium, on the acclimation, growth, and both the resulting polar and non-polar metabolic profiles (particularly on APD) of the microalgae *A. carterae* cultured in bench-scale bubble columns. The evaluation of bioactivities exhibited by the obtained methanolic extracts against relevant agricultural phytopathogens represents a significant advancement in the realm of sustainable microalgae-based pesticide production.

2. Materials and methods

2.1. Microalga and maintenance

The microalga *A. carterae* BMCC33 (in previous publications named Dn241EHU) deposited in the Basque Microalgae Culture Collection (Spain) was used. The inocula were cultivated in 175 cm^2 T-flasks with a working volume of 0.5L and acclimated to the f/2 medium formulation (Guillard. 1975) with a modified molar N/P ratio of 5 by adjusting the P concentration, and prepared in Mediterranean seawater. Nitrate was the nitrogen source (NO_3^--N). The culture medium underwent filtration for sterilization using a 0.22 µm filter. The flasks were subjected to a 12:12 h light–dark cycle and illuminated by 58 W fluorescent lamps, resulting in a surface irradiance of 60 µE $m^{-2} \cdot s^{-1}$ on the flasks. The pH of the culture medium was initially adjusted to 8.5 using HCl and NaOH solutions. The temperature was carefully maintained at a stable level of 21 ± 1 °C.

2.2. Culture experiments in photobioreactors

The cultivation of *A. carterae* was carried out in 10-L bench-scale photobioreactors using a bubble column configuration (BC-PBR) with sodium nitrate (coded as NIT), ammonium chloride (coded as AMO) and urea (coded as URE) as sole nitrogen sources at a nitrogen concentration of 2646 µM. BC-PBR were described elsewhere (López-Rosales et al., 2022). Aeration was implemented at a rate of 1 L min^{-1} (0.1 vvmin). For illumination purposes, light emitting diode (LED) strips (RGBWW) were carefully wound around the BC-PBR, providing a

uniform light intensity (600 $\mu E \cdot m^{-2} \cdot s^{-1}$ at the central region). The experimental setup involved a 12-hour light and 12-hour dark cycle, with the temperature maintained at a precise 20 ± 1 °C. To control the pH level of the environment, carbon dioxide injection was utilised, ensuring a constant pH of 8.5.

Growth media with each of the abovementioned nitrogen sources were prepared in Mediterranean seawater. The concentration of the f/2 formulation was tripled (f/2×3), maintaining the initial molar N/P ratio of 5. The potential for acclimation of *A. carterae* was investigated using sequential batch cultivation mode, starting with cells adapted to f/2 medium containing nitrate (see Section 2.1). The objective was to obtain cells acclimated to culture in BC-PBR under different nitrogen sources. To accomplish this, BC-PBR cultures began with an initial batch culture phase (named S1), in which 1 L of an inoculum containing cells in mid-linear growth phase was added to a 9 L fresh culture medium. The initial biomass concentration was of 32.44 ± 3.37 mg d.w. L^{-1}). A subsequent batch culture (named S2) was initiated by removing a variable volume of the culture and replacing it with an equal volume of fresh medium upon reaching the stationary growth phase. After measuring phosphate and nitrogen levels in the supernatant, the fresh medium was supplemented with phosphate and nitrogen stock solutions to achieve similar nutrient concentrations to the initial medium formulation throughout the culture volume (10 L). The remaining nutrients were also added in proportion to the selected medium formulation. Measurement of the maximum photochemical yield of photosystem II (F_V/F_M), which serves as an indicator of cell stress in microalgae, was carried out following a previously established procedure (López-Rosales et al., 2015). All experiments were run in duplicate.

2.3. Analytical measurements

The measurement of dry biomass concentration in the culture broth was periodically determined in triplicate from samples taken throughout the culture, as described earlier (Molina-Miras et al., 2018a). The concentrations of urea nitrogen (Urea-N), nitrate nitrogen (NO_3^--N), ammonium nitrogen (NH_4^+-N), total phosphorus (P_T) and nitrogen (N_T) in the

supernatants were determined as detailed elsewhere (Molina-Miras et al., 2020a). The biomass elemental composition (NOCHSP) was determined at the end of the subcultivation S2 (Molina-Miras et al., 2018a). Total lipid and carbohydrate contents were determined as described elsewhere (López-Rodríguez et al., 2020). A mean N-protein factor of 5.13 was used to calculate total protein concentration from total nitrogen content measurements in harvested biomass as recommended earlier for *A. carterae* (Lourenço et al., 2004). The identification and quantification of amphidinols (APD) were performed using NMR analysis of methanolic extracts obtained from the harvested biomass, following the procedures outlined in a previous publication (Abreu et al., 2019). Duplicate samples were analysed, and the average value was used.

2.4. Flow cytometric measurements

Flow cytometric measurements were conducted using a flow cytometer equipped with a blue light argon-ion excitation laser (488 nm) and three photomultiplier tubes (CellLabQuanta SC, Beckman Coulter Inc., Brea, CA, USA). Photomultiplier tubes included FL1 (525 nm band-pass), FL2 (575 nm band-pass), and FL3 (670 nm long-pass) to capture autofluorescence signals. The following characteristic parameters were quantified: mean autofluorescence intensity at specified wavelengths, cell concentration (N), and average equivalent cell diameter (D_e). Five measurements per sample were performed and an average value was used. At least 60 thousand cells were analysed per measurement. Equivalent cell volume was calculated as $\pi D_e^3/6$. The intrinsic fluorescence detected by FL3 and FL1-FL2 serves as an indicator for monitoring the cellular content of chlorophyll and carotenoids, respectively, when excited at a wavelength of 488 nm (Molina-Miras et al., 2020b). To facilitate comparison, the intensities of FL1, FL2, and FL3 were normalised relative to the average volume of the cells.

2.5. Determination of growth kinetic parameters

The biomass concentration (C_b) data over time (t) were fitted using the following logistic equation:

$$C_b(t) = x_o + \frac{x_1}{1+\exp\left(-\frac{t-x_2}{x_3}\right)} \quad (1)$$

where x_o, x_1, x_2, and x_3 are fit constants. The specific growth rate (μ, day^{-1}) was determined by calculating the rate based on the best fit curve obtained from Eq. (1) as follows:

$$\mu(t) = \frac{1}{C_b}\left(\frac{dC_b}{dt}\right) \quad (2)$$

The maximum specific growth rate, μ_{max} (day^{-1}), obtained from Eq. (2) was used. The biomass productivity at a given culture time, denoted as t, was determined as follows:

$$P_b = \frac{C_b - C_{bo}}{t} \quad (3)$$

The maximum values of P_b, P_{bmax}, were determined using Eq. (1) for C_b in Eq. (3). The biomass yield coefficients for nitrogen ($Y_{b/N}$) and phosphate ($Y_{b/P}$) were determined at the end of stage S2.

2.6. NMR spectra acquisition and data analysis

The preparation of the samples for NMR was performed as described earlier (Abreu et al., 2019). *A. carterae* freeze-dried biomass samples, obtained from the different culture phases S1 and S2 reached in PBR for each nitrogen source experiment, were extracted with two solvent systems: methanol (CD_3OD):water (D_2O) (80:20 v/v) and chloroform ($CDCl_3$):methanol (CD_3OD) (80:20 v/v). At least 4 biological replicates of biomass from each set were prepared with each solvent system. Five hundred microlitres of the supernatants were transferred to oven-dried 5 mm NMR tubes to be measured by ^{1}H NMR in a Bruker Avance III 600 spectrometer.

Statistical data analysis and multivariate modelling were carried out as described elsewhere (Abreu et al., 2019). In short, the resulting data matrices for each solvent system were combined and submitted to SIMCA-P software (v. 17.0, Umetrics, Sweden) for multivariate data analysis. ^{1}H NMR data was investigated by means of unsupervised techniques, Principal Component Analysis (PCA) and Hierarchical Cluster Analysis (HCA) and the supervised technique Partial Least Squares (PLS). Scaling was done to unit variance (UV) for all models. PLS models were validated using a permutation test with 100 permutations and validated by means of when the R^2 intercept does not exceed 0.4–0.5 and the Q^2 intercept does not exceed

0.05. Heatmaps were generated using the Statistical analysis tool in MetaboAnalyst 4.0 software (http://www.metaboanalyst.ca/). To generate the ^{1}H NMR data table for the heatmap, variable size bucketing of isolated peaks for each assigned metabolite in the spectra was performed and normalisation was done to total spectra intensity. Metabolite assignments were described elsewhere (Abreu et al., 2019). For univariate analysis, data was compared between two groups by the unpaired t-test, followed by multiple comparisons controlled by False Discovery Rate (FDR) method of Benjamini and Hochberg, and the fold-change (*FC*) values for each metabolite between two groups were calculated. The default criteria for screening differential metabolites were: VIP (variable importance in projection) > 1 for multivariate data analysis, and p (FDR) < 0.05 and $FC \geq 1.2$ or $FC \leq 0.83$ (i.e. changes of more than 20%) for univariate data analysis. Volcano diagram analysis and correlation analysis between the differential metabolites were performed applying the above-mentioned criteria.

2.7. Pathway analysis.

Pathway analyses were performed with MetaboAnalyst. The analyses utilised the global test algorithm for pathway enrichment and assessed metabolite importance through relative betweenness centrality. Pathways from Kyoto Encyclopedia of Genes and Genomes (KEGG) were used. MetaboAnalyst based its results on the pathways of the microalga *Chlorella variabilis*, the only microalgae database it has access to. The statistical results for each pathway include the p-values, Holm-adjusted p-values (using the Holm-Bonferroni method), FDR-adjusted p-values, and pathway impact indices. Pathways were deemed significantly enriched if the Holm p-value was less than 0.05, FDR was less than 0.05, and the impact was greater than 0.

KEGG microalgae-specific pathways were also used for interpretation purposes. KEGG organism-specific pathways contain entries representing genes or proteins present in the organism's genome. The absence of certain entries does not imply the absence of corresponding genes in the organism; it could be due to genes not being identified yet. *Symbiodinium minutum* (or *Breviolum minutum*) stands out among dinoflagellate microalgae as the only one in the

KEGG database with more comprehensive data available. When referencing information from KEGG microalgae, the species name will include the term "KEGG" enclosed in parentheses.

2.8. Anti-phytopathogenic activity assay

Antiphytopathogenic activity assays were carried out by Medina Foundation (Granada, Spain, https://www.medinadiscovery.com) using plant pathogen species from its own collection and protocols as described elsewhere (Audoin et al., 2013; Martinez et al., 2019). Samples consisted of crude extracts of *A. carterae* biomass obtained with methanol as the solvent. Six agricultural fungi (*Colletotrichum acutatum*, *Verticillium dahliae*, *Fusarium proliferatum*, *Fusarium cubense* TR4, *Botrytis cinerea*, *Magnaporthe grisea*) and one agricultural bacteria (*Clavibacter michiganensis* CECT790) were used. A concentration of 64 µg·mL^{-1} of raw algal extract was used in the protocol. This concentration is approximately 9-fold lower than the threshold value of 560 µg·mL^{-1} tested for activity detection by Audoin et al. (2013). Bioactivities were evaluated after 24 to 48 h. Measurements were carried out in duplicate samples and the average value was used.

2.9. Statistical analysis

A one-way analysis of variance (ANOVA) was conducted, followed by a post hoc test (Duncan's test), to assess potential differences between conditions, specifically regarding acclimation of cells to various nitrogen sources and progression of acclimation during subcultures (S1 to S2) for the same nitrogen source. The software used was Statgraphics Centurion XVIII (StatPoint, Herndon, VA, USA). Significant differences in the average response between treatments or subcultures were determined using a conservative significance level threshold of 1.0% (p-value < 0.01). Fisher's least significant difference (LSD) procedure was employed to distinguish between means at the 99.0% confidence level. Detailed explanations of the statistical analysis and multivariate modelling of NMR data can be found in Section 2.6.

Results and discussion

3.1. Photobioreactor cultures under different nitrogen sources.

In a recent study, *A. carterae* was shown to have the ability to acclimate to both combined and individual nitrogen sources, including nitrate, ammonium, and urea, over a wide range of concentrations (Molina-Miras et al., 2020a). The study was revelatory as it demonstrated the successful cultivation of a strain of the genus *Amphidinium* using urea as the sole nitrogen source, tolerating concentrations up to 5000 µM. However, experiments were carried out under culture conditions far from those used in PBR, i.e., small laboratory flasks, without stirring, pH control, or sparging. Therefore, a proof of concept performed in photobioreactors was needed to demonstrate the scalability of the previous results. Thus, in this work, *A. carterae* was cultured in batch mode in 10L CB-PBR under three sole nitrogen sources (nitrate, culture coded as NIT; urea coded as URE; and ammonium coded as AMO) according to Section 2.2. Intriguingly, the inoculum of *A. carterae* had previously been maintained in T-flasks (see Section 2.1.) over a long period (> 2 years) in f/2 medium (with 882 µM NO_3-N as the sole nitrogen source). Therefore, the dynamics of acclimation from inoculum conditions to those of each BC-PBR was interpreted based on different kinetic parameters described above in Sections 2.3, 2.4, and 2.5.

Figure 1 shows the temporal evolution of *A. carterae* growth, the concentrations of available macronutrients in the supernatants, and the cytometric measurements of the cells in each photobioreactor. During the first batch culture (stage S1), all nitrogen sources were consumed by the cells, leading to similar increases in cell concentration in the different CB-PBR. However, variations in the biomass concentration kinetics occurred as a result of disparities in cell size between nitrogen sources. As can be appreciated in Figs. 1A, 1C and 1E, nitrate, urea, and ammonium were already depleted in the stationary phase of stage S1, while phosphate remained in excess. Therefore, the stoichiometry of growth was governed by the availability of nitrogen in the culture broth.

Interestingly, unlike URE (Fig. 1D) and AMO (Fig. 1F), the average mean florescence intensities FL1, FL2, and FL3, relative to cell biovolume, barely changed for NIT (Fig. 1B) in stage S1. These signals, related to the cellular pigment profile (Molina-Miras et al., 2020b), have proven to be an effective tool for assessing cellular responses to acclimatization processes or

toxicity (Molina-Miras et al., 2020a; Seoane et al., 2021). Therefore, this observation supports the idea that cells were acclimated to nitrate as the primary nitrogen source from the beginning of the culture in NIT. The most significant fluctuations in FL1-3 were observed in the exponential phase of AMO, followed by UREA, and gradually decreased as the cultures approached the stationary phase of the S1 stage.

BC-PBR were subcultured (stage S2) using cells from S1 cultures as inoculum (see Fig. 1). During S2, the range of variation of the relative FL1-3 values in NIT was small and similar to that recorded in S1. In the case of URE, the FL1-3 values exhibited minimal changes compared to those observed during acclimation in S1, with values falling within the same range as those measured for NIT. On the contrary, acclimation was unattainable in the case of AMO. NH_4^+-N-related toxicity became evident, as at the end of the stage S2, there were hardly any intact cells ($<2.5\times10^4$ cells mL^{-1}) all of which exhibited significantly high FL1-3 values. These observations are consistent with those reported earlier for *A. carterae* grown in T-Flaks, which indicated a tolerance concentration threshold of NH_4^+-N 441 µM (Molina-Miras et al., 2020a). Indeed, this threshold value is well below the initial ammonium concentration used in the CB-PBR culture (2646 µM NH_4^+-N). Concomitantly, the impact of ammonium toxicity also became evident through a significant reduction in the F_V/F_M value in cells (0.26 ± 0.02 in stage S2). In contrast, *Fv/Fm* did not change significantly with average values of 0.50 ± 0.10 and 0.53 ± 0.11 for NIT and URE, respectively, indicative of healthy cells (Molina-Miras et al., 2020a).

Figure 2 summarises the effect of the nitrogen source on typical kinetic parameters of culture performance in photobioreactors: μ_{max}, P_{bmax}, $Y_{b/N}$ and $Y_{b/P}$. The values used correspond to the end of the S2 subculture, at which point the acclimation process to the nitrogen source could be considered completed. A one-way ANOVA was performed at the 1% significance level for each kinetic parameter determined in Fig. 2. For all four parameters, multiple range tests determined two homogeneous groups: one of them composed of AMO and the other by URE and NIT. As mentioned above, the initial concentration of ammonium in each subculture was toxic for *A. carterae*. There was no statistically significant difference between the mean values of the kinetic parameters for URE and NIT: μ_{max} = 0.30 ± 0.08 day^{-1}; P_{bmax} = 43 ± 8 $mg{\cdot}L^{-1}{\cdot}day^{-1}$;

$Y_{b/N}$ = 9.1 ± 0.6 g biomass d.w. g^{-1} N; $Y_{b/P}$ = 7.1 ± 0.1 g biomass d.w. g^{-1} P. This observation reinforces previous findings in which the concurrent removal by *A. carterae* of dissolved nitrate and urea in a culture medium was successfully showcased (Molina-Miras et al., 2020a). In fact, the values of the above parameters are of the same order as those reported in other studies for *A. carterae* cultured in nitrate-fed PBR (López-Rosales et al., 2022; Molina-Miras et al., 2020b, 2018a). To our knowledge, this is the first evidence of urea-N-supported growth in bench-scale photobioreactors for *Amphidinium* species, confirming previous results obtained in small flasks (Molina-Miras et al., 2020a). According to these results, substitution of nitrate as a nitrogen source by a greener source such as urea in industrial-scale PBR cultures would be feasible in multi-product microalgae-based biorefineries at least for *A. carterae*.

The available literature does not provide specific information on the characteristics of the dinoflagellate *Amphidinium* that contribute to its high tolerance to urea. Certain microalgae groups, including dinoflagellates, that thrive in eutrophic waters are believed to have developed adaptative mechanisms to efficiently uptake and tolerate high nitrogen concentrations (Molina-Miras et al., 2020a). These mechanisms probably contribute to their ability to flourish in environments rich in nutrients, including urea. Further research is needed to investigate and understand these specific traits. In any event, the level of tolerance to urea depends on species and strains (Solomon et al., 2010). Therefore, each strain must be studied in depth.

3.2. Comparative metabolomic NMR analysis.

Urea can displace nitrate as a source of nitrogen in the mass cultivation of *A. carterae* in PBR, as show in the section above. However, fine biochemical monitoring is needed. (Abreu et al., 2019), Using untargeted NMR-based metabolomics, potential biomarkers of cells acclimated to urea relative to nitrate may be identified. NMR may provide insights into the relationship between microalgal metabotypes and the nitrogen sources used in PBR cultures. Thus, extracts of *A. carterae* from biomass harvested in the two stationary phases (S1 and S2), both reached in the NIT and URE PBR cultures (coded as NIT-S1, URE-S1, NIT-S2 and URE-S2, respectively), were analysed by ^{1}H NMR.

An evaluation of the ^{1}H NMR data set was performed by PCA and HCA. The PCA score plot of the first two principal components (PC1 and PC2) explains 90.4% of the total variance (see Supplementary Materials). A noticeable discriminatory pattern was observed, indicating metabolic differentiation between the four different experimental sets. The PCA score plot revealed three distinct groups: (i) that formed by both nitrogen sources in the pre-acclimation stage (NIT-S1 and URE-S1), which will be referred to as group NUS1; and (ii) two independent groups corresponding to the cultures acclimated in stage S2 (NIT-S2 and URE-S2). In PC1, NIT-S2 was clearly separated from the others, while PC2 was more relevant in the separation of URE-S2 from the other treatments. The NUS1 group was expected since both NIT-S1 and URE-S1 corresponded to two metabolic transition states given in batch cultures that started with cells acclimated to the same conditions (see Section 2.1) but exposed to different nitrogen sources. The transition to acclimation to each nitrogen source led to different microalgal metabotypes for cells in NIT-S2 and URE-S2. The observations were further corroborated with greater precision through the HCA plot, since it effectively grouped the NIT-S1 and URE-S1 samples, while distinctly highlighting the pronounced dissimilarity between NIT-S2 and URE-S2 samples (see Supplementary Materials).

Similarly, to gain a thorough understanding of the metabolic variations between the three different groups established above, a hierarchically clustered heat map (Fig. 3A) was obtained from a total of 43 ^{1}H NMR normalised bins containing the assigned metabolites. Fig. 3A unambiguously indicates that metabolite expression levels significantly differ among the three groups (NUS1, NIT-S2, and URE-S2). According to PCA, HCA, and heatmap, the most interesting comparisons would be the following. In NIT-S1 vs NIT-S2, cells from the inoculum were already acclimated to nitrate. Therefore, the comparison aims to reveal metabolic changes in stationary phase cells during acclimation to photobioreactor culture (i.e., a 1:20 scale change from static 0.5 L T-flasks to 10 L BC-PBR; bubbling and pH control, etc.) after two repeated batch cultures. The comparison URE-S1 vs URE-S2 accounts for acclimation to urea but coupled to that of the photobioreactor (given by NIT-S1 vs NIT-S2). Finally, the comparison NIT-S2 vs URE-S2, in which the photobioreactor effect is expected to be uncoupled after two sub-cultivations in BC-

PBR, is the main factor contributing to the differentiation between metabolic changes by acclimatization to urea and nitrate. For the sake of brevity and greatest impact, only the results from NIT-S2 vs URE-S2 will be discussed below.

The nitrogen source significantly influenced the gross biochemical composition of the dry biomass. URE-S2 had protein, lipid and carbohydrate contents of 39.5 ± 0.7%, 14.5 ± 0.5%, and 42.4 ± 0.4%, respectively, while NIT-S2 had contents of 27.9 ± 1.3%, 17.5 ± 0.4%, and 48.1 ± 2.0%, respectively. These values fall within the reported ranges for microalgae: 28-70% for protein, 10-20% for lipids, and 10-50% for carbohydrates (Yaakob et al., 2021). The effects of urea and nitrate as nitrogen sources on the gross biochemical composition of microalgae are highly dependent on the specific microalgae species involved (Lourenco et al., 2002), adding complexity to the understanding of their influence.

In terms of specific metabolites, the biomass from the nitrate-fed PBR culture (particularly NIT-S2; Fig. 3A) exhibited a marked general increase in free amino acids (for example, alanine, threonine, valine, isoleucine, leucine, lysine, glutamine, proline, asparagine, tyrosine, phenylalanine, and tryptophan). Similarly, the levels of fatty acids (except ω-3), organosulfur acids (betaine, dimethylsulfoniopropinate and sarcosine) and organic carboxylates (acetate, acetoacetate, and pyruvate), nucleosides (uridine and uracil), hormones (oxylipins) and carotenoids (peridinin) increased. Interestingly, the levels of carbohydrates α-galactose and β-glucose were higher in NIT, while their isomers β-galactose and α-glucose were higher in URE. Lastly, maximum production peaks of APD, EPA, DHA, ω-3 fatty acids, unsaturated fatty acids (UFA), triacylglycerols (TAG), glycerol, quaternary ammonium compounds (choline and derivatives) and glutamate amino acid were detected at higher concentrations in urea-fed PBR cultures. It should be noted that NMR metabolomics allowed the simultaneous determination of all these metabolites from a single 1H NMR spectrum, typically acquired in less than a minute. This capability provides solid evidence that this technique can guide the development of superior cultivation strategies, opening new avenues for improved microalgal refinement.

Regarding the differentiation of the second batch culture, a PLS-DA model was generated from NIT-S2 and URE-S2. A clear separation was observed between the NIT-S2

411 metabolites from those of URE-S2. The cumulative values of R^2 (0.976) and Q^2 (0.999)
412 demonstrated the excellent fitness and predictive accuracy of the model (see Supplementary
413 Materials). With a Q^2 value of almost 1, the existing distribution of data points would encompass
414 any additional sample incorporated into the model, indicating that the model is highly resilient
415 and capable of accurately explaining the dissimilarities between the two sample sets without
416 overfitting the data.

417 Figure 3B compares URE-S2 versus NIT-S2 based on FC values of the up-regulated and
418 down-regulated metabolites and their level of significant difference on the ordinate axis. The
419 bubble chart in Figure 3C displays the enrichment pathways for URE-S2 versus NIT-S2, with
420 each bubble representing a metabolic pathway. The switch from nitrogen source to urea had a
421 significant impact on free amino acids, except for aspartate (Fig. 3B). Eleven amino acids,
422 including alanine, glutamine, isoleucine, leucine, lysine, phenylalanine, tryptophan, tyrosine,
423 valine, threonine, and proline, were down-regulated. Glutamate was the only amino acid that
424 was up-regulated, but weakly. Interestingly, the protein content of the biomass harvested in
425 URE-S2 was 42 % higher than in NIT-S2. These findings indicate that the tuning of the nitrogen
426 source, in this case to urea, led to an increase in protein production, as reported for other
427 microalgae (Batista et al., 2019; Fatini et al., 2021; Ribeiro et al., 2020), compatible with an
428 increased protein to amino acid ratio as observed in *Chlamydomonas reinhardtii* when urea and
429 ammonium were compared as nitrogen sources (Batista et al., 2019).

430 Then, the statistically affected pathways involved in amino acid metabolism was
431 analysed from the KEGG database for dinoflagellates including *Symbiodinium minutum*. Each
432 pathway is presented in descending order of impact, along with the dysregulated metabolites,
433 the enzymes whose genes encoding them were found, and the reactions that they catalyse
434 within the pathway; abbreviations from the legend of Fig.3A were used. **(1)** Phenylalanine,
435 tyrosine and tryptophan biosynthesis (*phe, tyr*, *trp*); tryptophan synthase (indoleglycerol
436 phosphate ↔ *trp*); aromatic amino acid aminotransferase I / 2-aminoadipate transaminase (3-
437 (4-hydroxyphenyl)pyruvate → *tyr*). **(2)** Arginine and proline metabolism (*pro*); pyrroline-5-
438 carboxylate reductase (*pro* ↔ 1-pyrroline-5-carboxylate) and prolyl 4-hydroxylase (*pro* ↔

hydroxyproline). **(3)** Tryptophan metabolism (*trp*); five enzymes (*trp* → indole pyruvate, N-formul-kynurenine; tryptamine, indole pyruvate → *trp*. **(4)** Tyrosine metabolism (*tyr*, *acetoacetate*); the same enzyme for *tyr* than pathway (1); genes that encode the production of *acetoacetate* are not reported for *S. minutum* and dinoflagellates (KEGG). **(5)** Valine, leucine, and isoleucine biosynthesis (*val*, *leu*, and *ile*); branched-chain amino acid minotransferase (intermediates → *val*, *leu, ile*). **(6)** Arginine biosynthesis (*asp*, *gln*); glutamine synthetase (NH_3 → *gln*); genes encoding aspartate conversion are not reported in KEGG for *S. minutum* and dinoglagellates. **(7)** Alanine, aspartate, and glutamate metabolism (*ala*, *asp*, *glu*); alanine transaminase (*ala* ↔ *pyr*); asparagine synthase (*asp* ↔ asparagine); glutamine synthetase (*glu* → *gln*); 1-pyrroline-5-carboxylate dehydrogenase (*glu* → 1-pyrroline-5-carboxylate).

The observed pattern described above strongly implies a predominance of protein anabolism, that is, the intricate process of synthesising complex organic molecules from simpler ones, over catabolism, which involves the breakdown of proteins into amino acids and other simple derivative compounds (Batista et al., 2019). In this scenario, biomass stoichiometry may be an interesting marker. Thus, while the average P-molar formula for NIT-S2 was $C_{53.9}$ $O_{28.5}$ $H_{102.8}$ $N_{5.2}$ $S_{0.4}$ P_1, that of URE-S2 was $C_{53.6}$ $O_{25.6}$ $H_{99.6}$ $N_{7.2}$ $S_{0.5}$ P_1. This difference in the P-molar formulas between the nitrate-fed and urea-fed cultures implied variations in elemental ratios and possibly in the availability of key elements for protein synthesis. Specifically, the molar C:N ratio of NIT-S2 (10.4) was higher than that of URE-S2 (7.4), which follows the reported trends for the dinoflagellate microalgae *Prorocentrum donghaiense* grown under urea or nitrate replete conditions (Jing et al., 2017). The higher carbon content compared to nitrogen in NIT-S2 suggests an imbalance in biomass stoichiometry, which may affect nitrogen availability for protein synthesis and impact the efficiency of protein anabolism in that culture. Jing et al. (2017) also found that the urea transporter gene was highly responsive to changes in urea concentration, while other genes related to nitrogen transport and metabolism are more sensitive to changes in general nitrogen availability. This differential responsiveness is linked to biomass stoichiometry and protein anabolism, as it reflects the organism's ability to adapt its

nitrogen utilisation strategy based on the availability of different nitrogen sources. This adjustment in gene expression may influence the efficiency and extent of protein synthesis.

Regarding fatty acids, monounsaturated fatty acids (MUFA) and PUFA, particularly long-chain ω-3 fatty acids such as EPA and DHA, were up-regulated (Fig. 3B). The remaining FAs, which are mainly saturated and of short chain, were down-regulated. These results allow hypothesising about the presence of specific genes, regulated through urea as a nitrogen source, that could have the potential to significantly enhance the production of n-3 PUFA in *A. carterae*. The latter statement is supported by recent literature in which *Thraustochytriidae* sp benefits from sodium nitrate as a nitrogen source for the accumulation of short-chain fatty acids, while urea is advantageous for n-3 PUFA biosynthesis of n-3 (Li et al., 2020). In fact, cultivation with urea resulted in the up-regulation of several key genes associated with the synthesis of long chain fatty acids, while cultivation with sodium nitrate resulted in an increase in nitrate reductase (Li et al., 2020). The changes described above are consistent with the significant observed alterations in pyruvate **(8)** and glycerophospholipid **(9)** metabolisms observed (Fig. 3C); the first characterised by down-regulation of acetate and the second by up-regulation of choline and choline phosphate. Both metabolisms are involved in the direct modification of the fatty acid profile in cells (Santin et al., 2021). Genes encoding enzymes that catalyse the conversion of these metabolites were not reported in KEGG for dinoflagellates, unlike diatoms.

It is important to note that amphidinols (APD) were the most up-regulated metabolite family (Fig. 3B). Isoquinoline alkaloid biosynthesis (**10**) (Fig. 3C) was significantly affected by downregulation of tyrosine. This pathway is typically found in higher plants (Desgagne´-Penix, 2021), but not in microalgae. Both isoquinolines and APD are secondary metabolites, but isoquinolines are alkaloids, while APD are polyketides (macrolides) produced by polyketide synthase (PKS) pathways that use acyl-CoA precursors. Genes encoding enzymes involved in the conversion of tyrosine to the intermediate 3-(4-hydroxyphenyl)pyruvate have been reported for the group dinoflagellates (KEGG), but not for *S. minutum* (KEGG). It is intriguing to speculate that tyrosine may serve as a precursor in PKS pathways responsible for APD production in *A. carterae*. However, ongoing research is being conducted to elucidate the potential role of

tyrosine as a marker for APD biosynthesis, due to uncertainties regarding the presence of specific genes regulated by urea as a nitrogen source. If this pathway is indeed conserved in *A. carterae*, it is highly likely that it contributes to the synthesis of macrolides rather than alkaloids, which, to the best of our knowledge, have not been reported in *Amphidinium*.

Another series of metabolites were also detected as responsible for the changes observed in the different pathways (see Fig. 3C). Uridine, uracil, and glutamine appeared as markers in pyrimidine metabolism (**11**). *S. minutum* (KEGG) presents genes encoding enzymes of this pathway: (i) carbamoyl-phosphate synthase (gln → carbamoyl phosphate); (ii) uridine kinase (*urid* → uridylic acid); and (iii) pseudouridylate synthase (pseudouridine 5'-phosphate ↔ *uracil*).

Glutathione metabolism (**12**) was also affected by up-regulation of glutamate. *S. minutum* (KEGG) presents genes encoding different critical enzymes of this pathway: (i) gamma-glutamylcysteine synthetase for the conversion of the precursor L-glutamate to the intermediate gamma-L-glutamyl-L-cysteine, which ultimately is transformed into glutathione by the action of the enzyme glutathione synthase; and (ii) one fraction of the formed glutathione is converted again into L-glutamate by the action of glutathione transferase, gamma-glutamyltranspeptidase and glutathione hydrolase. It is worth recalling that glutathione serves as a key metabolite for the regulation of oxidative stress in microalgae, and therefore the impact of urea compared to nitrate on this pathway remains unknown. Understanding the physiological significance of glutathione in microalgae is hindered by the lack of information about the genes responsible for its synthesis (Tamaki et al., 2021).

The group of metabolites formed by the natural metabolic activity of acetate and glutamine was identified as down-regulated within glyoxylate and dicarboxylate metabolism (**13**). While *S. minutum* (KEGG) has genes encoding the acetyl-CoA synthetase responsible for the conversion of the precursor internal acetate to Acetyl-CoA, no enzyme has been reported for the conversion of glutamine in this pathway for dinoflagellates (KEGG). On the contrary, while glutamate synthetase has been reported in KEGG for diatoms, pelagophytes, haptophytes, green algae, and red algae, it has not been reported for eustigmatophytes. This suggests a strong likelihood of the widespread presence of this enzyme in microalgae.

Regarding α-glucose (up) and acetate (down) in Glycolysis/Gluconeogenesis (**14**), α-glucose is converted to α-glucose-6P by a reaction mediated by the enzyme glucokinase. Acetyl-CoA synthetase catalyses the conversion of internal acetate to Acetyl-CoA (as in pathway 13). With respect to aspartate (down) and alanine (down) in carbon fixation in photosynthetic organisms (**15**), genes encoding the enzyme alanine transaminase, responsible for catalysing the conversion of alanine to pyruvate, have been reported in dinoflagellates according to KEGG. However, aspartate-converting enzymes have not been found in dinoflagellates according to KEGG, but have been identified in other microalgae.

Current studies on dinoflagellates and other microalgae which have identified genes responsible for transporting urea, compared to those involved in transporting nitrates, are scarce. This knowledge gap is important to understand the dysregulation of markers in these pathways, and further research is necessary to uncover the molecular mechanisms underlying these processes and improve the understanding of these important biological pathways.

3.3. Correlation of amphidinols with bioactive metabolites

As mentioned above, *A. carterae* shows great potential as a source of compounds with pesticide activity, particularly amphidinols (APD). In addition, it can also produce other valuable bioactive products, such as PUFA (e.g., EPA and DHA) and carotenoids (e.g., peridinin). NMR metabolomics, a proven strategy, not only offers the ability to estimate the concentration of targeted metabolites but also reveals correlations between numerous metabolites, providing valuable insights into their interplay and biological roles when enhanced or reduced. Hence, rapid and reproducible monitoring is crucial to identify the bioactive compounds that are associated with APD production. For this purpose, NMR is employed as a key tool for gaining deeper insights into the synthesis of these metabolites in *A. carterae*.

In this sense, to clarify which bioactive metabolites significantly increased or decreased along with the increased content of APD, a PLS analysis was performed. Figure 4A displays the PLS score scatter plot showing the complete separation of the metabolite profiles of *A. carterae* in urea-fed (URE-S2) and nitrate-fed (NIT-S2) PBR cultures. The discriminating vector T[1]

accounted for the most significant variation in the dataset, followed by the T[2] vector, with the scores of each vector being completely independent (orthogonal) to one another. The loading plot in Figure 4B provides a visual representation of the buckets that have higher correlations, whether positively or negatively, to those of the APD, which are, respectively, the closest (blue points) and furthest (red point) to the green point representing the APD bucket. Figure 4C shows the contribution plot with the markers highlighted in Fig. 4B. Thus, choline-based compounds, DHA, EPA, *α*-glucose and glutamate increased with increasing APD content, while peridinin was found to decrease.

Establishing a relationship between α-glucose, glutamate, and peridinin with APD is challenging due to its complexity, whereas between both DHA and EPA with APD is plausible. According to Remize et al. (2020), the Polyketide Synthase (PKS) pathway offers an alternative route to produce n-3 PUFA in dinoflagellates, in which PKS enzymes exhibit different configurations, leading to different types of PKS. Dinophytes have been found to possess Type I and Type II PKS, where the former comprises a large multifunctional enzyme with all catalytic domains on a single peptide, whereas the latter consists of mono-functional enzymes with a single catalytic domain. Dinoflagellates are believed to employ both the conventional pathway and the PKS pathway to synthesise EPA and DHA. Interestingly, the PKS pathway has also been associated with the biosynthesis of polyketides in dinoflagellates, and as APD are polyketides, this suggests a close relationship between APD production and PUFA synthesis in *A. carterae*. This correlation is further supported by the potential presence of specific genes in *A. carterae*, which are likely regulated by urea as a nitrogen source and stimulate the production of n-3 PUFA (as described above). Consequently, it is expected that the APD-to-nitrogen yield coefficient ($Y_{APD/N}$) for URE might increase in comparison to that for NIT. Calculations supported the latter statement, revealing that the $Y_{APD/N}$ value derived from urea-fed BC-PBR cultivation (135±4 mg/g) was approximately 2.5 times higher than that observed in the nitrate-fed BC-PBR culture (55 ± 1 mg/g).

3.4. Revealing antiphytopathogenic extracts from A. carterae for sustainable agriculture

Figure 4D illustrates the results obtained from the anti-phytopathogenic activity of crude methanolic extracts derived from biomass harvested in NIT-S2 and URE-S2. These extracts were evaluated against a panel of six agricultural fungi (*C. acutatum, Verticillium dahliae, Fusarium proliferatum, Fusarium cubense TR4, Botrytis cinerea, Magnaporthe grisea*) and one agricultural bacteria (*Clavibacter michiganensis CECT790*). The most remarkable results were observed with URE-S2 extracts, demonstrating robust antiphytopathogenic effects with an approximate 100% inhibition of growth against the six fungal types tested. Furthermore, these extracts exhibited moderate to low activity, approximately 20% inhibition of growth, against the bacterium *C. michiganensis*. Similar results were observed for NIT-S2 extracts, except *Fusarium* genus fungi, which showed notably low antiproliferative activity (<10% inhibition of growth).

Previous studies (Echigoya et al., 2005; Thomas et al., 2022; Navarro López et al., 2023) have reported the antifungal activity of extracts derived from *A. carterae* due to the prominent role of APD. A comprehensive life cycle assessment of an agricultural fungicide based on amphidinols produced by *A. carterae* has recently been reported (López-Herrada et al., 2023). The study found that this microalgae-based fungicide offers a viable and sustainable alternative to traditional fungicides, with the potential for improved economics through optimised cultivation conditions and low-cost nutrient sources. The environmental impact of microalgae cultivation, in particular the use of fertilisers, was also addressed. In this sense, it is recognised that the cost of fertiliser can vary depending on factors such as region, market conditions and availability, but urea-based fertilisers are generally considered to be more cost effective due to their wider production and lower manufacturing costs.

Interestingly, the results presented here suggest that the profile of APD in biomass may differ depending on the nitrogen source used, as evidenced by the increased activity of URE-S2 against two strains of the *Fusarium* genus compared to NIT-S2. This hypothesis is supported by previous findings. For instance, studies have demonstrated intraspecific variation in the APD profile of strains of *A. carterae*, with nine different amphidinol analogs detected in A. carterae BMCC33 (Wellkamp et al., 2020). The quantitative expression of APD in *A. carterae* BMCC33 has shown varying cell quotas for each analog. Furthermore, it has been reported that the activity of

each analog can differ according to its structure (Wellkamp et al., 2020). Similar observations have been made with structurally related karlotoxins produced by species of *Karlodinium*, where nutrient availability has been shown to influence their profile (Bachvaroff et al., 2009). Therefore, the composition or characteristics of the nitrogen source have the potential to affect the APD profile, which in turn may impact its bioactivity. Further extensive research is required to fully validate this hypothesis. Regardless of the above, antiphytopathogenic extracts sourced from urea-fed photobioreactor cultures represent a potential environmentally friendly solution for disease management in crop production, which has been unexplored previously in the context of implementing NMR metabolomics as an integrated strategy towards the refinement for a superior cultivation.

3.5. Future prospects

The public's preference for eco-friendly and sustainable agricultural practises has driven the demand for novel agrochemicals as alternatives to synthetic pesticides. Microalgae, known for their potential to produce compounds with antimicrobial and toxic properties, represent a technological challenge for researchers in the development of biopesticides. Research on microalgal metabolic pathways and the mechanisms of action associated with these metabolites remains limited. Therefore, there is a need to further investigate the use of secondary metabolites derived from microalgae, including microalgal biomass, as a promising option to replace chemical pesticides (Costa et al., 2019). On the opposite side, the use of microalgae biomass for human applications often faces limitations or concerns when cultivated in wastewater. To overcome this drawback, the use of chemically defined culture media is considered an alternative solution, with the requirement that their components are sourced from sustainable sources. An example is based on the use of urea as a nitrogen source to produce APD by means of cultures of *A. carterae*.

Further research is needed to replace all components of a growth medium with sustainable sources. This task can be challenging due to intra- and inter-species variation and the expected impact on the cell metabolome. In this context, the application of NMR

metabolomics is emerging as a suitable approach to accompany this critical step of microalgae-based bioprocesses. As NMR sensitivity and line resolution continue to improve with the development of new cryoprobe development and magnetic field instrumentation, it will play a crucial role in the development of sustainable and efficient microalgae cultivation systems, particularly in the design of customised and chemically defined culture media, allowing the production of high-value compounds with minimal environmental impact. NMR metabolomics would guide advanced cultivation strategies for improved microalgal refinement, biomass productivity, and targeted biomolecule production.

4. Conclusions

For the first time, urea as a sustainable nitrogen source was shown to allow robust growth of *A. carterae* in photobioreactors. Nitrogen availability dictated the growth stoichiometry, with NH_4^+-N-related toxicity observed. Substitution of nitrate with urea in large-scale photobioreactors shows promise for multiproduct microalgae-based biorefineries. NMR-based metabolomics revealed nitrogen source-dependent metabotypes and significant changes in the metabolic profile, which could be unraveled by means of down- and up-regulated compounds, with a clear correlation between amphidinol production and PUFA synthesis. Extracts from urea-fed cultures exhibited potent antiphytopathogenic activity against agricultural phytopathogens, highlighting their potential for sustainable pesticide development.

E-supplementary data of this work can be found in e version of this the paper online.

Acknowledgements

This work has been funded by the State Research Agency (grants PID2019-109476RB-C22, PLEC2021-007774, PDC2021-121248-I00, PID2021-126445OB-I00 and RTC-2017-6405-1) of the Spanish Ministry of Science, Innovation and Universities; the General Secretariat of Universities, Research and Technology of the Andalusian Government (grant: P18-RT-2477); and the European Regional Development Fund Program. We would also like to thank Dr. Fernando

Reyes, Area Head- Chemistry, Fundación Medina (Granada, Spain), who carried out the agriculture phytopathogens assays. Ana C. Abreu thanks to University of Almería for her Hipatia scholarship (E-04-2020-0098122).

References

1. Abreu, A.C., Molina-Miras, A., Aguilera-Sáez, L.M., López-Rosales, L., Cerón-García, M.C., Sánchez-Mirón, A., Olmo-García, L., Carrasco-Pancorbo, A., García-Camacho, F., Molina-Grima, E., 2019. Production of amphidinols and other bioproducts of interest by the marine microalga *Amphidinium carterae* unraveled by nuclear magnetic resonance metabolomics approach coupled to multivariate data analysis. J. Agric. Food Chem. 67, 9667−9682.
2. Audoin, C., Bonhomme, D., Ivanisevic, J., de la Cruz, M., Cautain, B., Monteiro, M. C., Reyes, F., Rios, L., Perez, T, Thomas, O. P. 2013. Balibalosides, an original family of glucosylated sesterterpenes produced by the Mediterranean sponge *Oscarella balibaloi*. Marine drugs, 11(5), 1477-1489.
3. Bachvaroff, T. R., Adolf, J. E., Place, A. R., 2009. Strain variation in *Karlodinium veneficum* (dinophyceae): toxin profiles, pigments, and growth characteristics 1. J. Phycol. 45(1), 137-153.
4. Barone, M.E., Murphy, E., Parkes, R., Fleming, G.T.A., Campanile, F., Thomas, O.P., Touzet, N., 2021. Antibacterial Activity and Amphidinol Profiling of the Marine Dinoflagellate *Amphidinium carterae* (Subclade III). Int. J. Mol. Sci. 22, 12196.
5. Batista, A.D., Rosa, R.M., Machado, M., Magalhães, A.S., Shalaguti, B.A., Gomes, P.F., Covell, L., Vaz, M.G.M.V., Araújo, W.L., Nunes-Nesi, A., 2019. Increased urea availability promotes adjustments in C/N metabolism and lipid content without impacting growth in *Chlamydomonas reinhardtii*. Metabolomics 15, 1−14.
6. Behera, B., Venkata Supraja, K., Paramasivan, B., 2021. Integrated microalgal biorefinery for the production and application of biostimulants in circular bioeconomy. Bioresour. Technol. 339, 125588.

7. Costa, J. A. V., Freitas, B. C. B., Cruz, C. G., Silveira, J., & Morais, M. G. (2019). Potential of microalgae as biopesticides to contribute to sustainable agriculture and environmental development. J. Environ. Sci. Health B, *54*(5), 366-375.
8. Desgagné-Penix, I. Biosynthesis of alkaloids in Amaryllidaceae plants: a review, 2021. Phytochem. Rev. 20, 409–431.
9. Echigoya, R., Rhodes, L., Oshima, Y., Satake, M., 2005. The structures of five new antifungal and hemolytic amphidinol analogs from *Amphidinium carterae* collected in New Zealand. Harmful Algae 4, 383–389.
10. Fatini, M.A., Basri, E.M., Wan Maznah, W.O., 2021. Effect of different nitrogen sources on cell growth and biochemical compositions of *Chlorococcum* sp. cultivated under laboratory conditions. IOP Conf. Ser. Earth Environ. Sci. 711, 012010.
11. Guillard, R.R.L., 1975. Culture of phytoplankton for feeding marine invertebrates, in: Smith, W.L., Chanley, M.H. (Eds.), Culture of Marine Invertebrate Animals. Springer, Boston, MA, pp 29–60.
12. Jing, X., Lin, S., Zhang, H., Koerting, C., Yu, Z., 2017. Utilization of urea and expression profiles of related genes in the dinoflagellate *Prorocentrum donghaiense*. PLoS One 12(11), e0187837.
13. Kim, H., Choe, C., Lee, A., & Lim, H., 2023. Application of green hydrogen with theoretical and empirical approaches of alkaline water electrolysis: Life cycle-based techno economic and environmental assessments of renewable urea synthesis. Int. J. Hydrog. Energy, 48(43), 16148-16158.
14. Kumar, A., Bera, S., 2020. Revisiting nitrogen utilization in algae: A review on the process of regulation and assimilation. Bioresour. Technol. Rep. 12, 100584.
15. Li, K., Liu, Q., Fang, F., Luo, R., Lu, Q., Zhou, W., Huo, S., Cheng, P., Liu, J., Addy, M., Chen, D., Ruan, R., 2019. Microalgae-based wastewater treatment for nutrients recovery: A review. Bioresour. Technol. 291.
16. Li, S., Hu, Z., Yang, X., Li, Y., 2020. Effect of nitrogen sources on omega-3 polyunsaturated fatty acid biosynthesis and gene expression in *Thraustochytriidae* sp. *Mar. Drugs 18*(12), 612.

17. López-Herrada, E., Gallardo-Rodríguez, J. J., López-Rosales, L., Cerón-García, M. C., Sánchez-Mirón, A., & García-Camacho, F., 2023. Life-cycle assessment of a microalgae-based fungicide under a biorefinery approach. Bioresour. Technol., 129244.
18. López-Rodríguez, M., Cerón-García, M. C., López-Rosales, L., Navarro-López, E., Sánchez-Mirón, A., Molina-Miras, A., Abreu, A. C., Fernández, I., García-Camacho, F. 2020. Improved extraction of bioactive compounds from biomass of the marine dinoflagellate microalga *Amphidinium carterae*. Bioresour. Technol., *313*, 123518.
19. López-Rodríguez, M., Cerón-García, M.C., López-Rosales, L., Navarro-López, E., Sánchez Mirón, A., Molina-Miras, A., Abreu, A.C., Fernández, I., García-Camacho, F., 2021. An integrated approach for the efficient separation of specialty compounds from biomass of the marine microalgae *Amphidinium carterae*. Bioresour. Technol. 342., 125922.
20. López-Rosales, L., García-Camacho, F., Sánchez-Mirón, A., Contreras-Gómez, A., Molina-Grima, E., 2015. An optimisation approach for culturing shear-sensitive dinoflagellate microalgae in bench-scale bubble column photobioreactors. Bioresour. Technol. 197, 375–382.
21. López-Rosales, L., López-García, P., Benyachou, M.A., Molina-Miras, A., Gallardo-Rodríguez, J.J., Cerón-García, M.C., Sánchez Mirón, A., García-Camacho, F., 2022. Treatment of secondary urban wastewater with a low ammonium-tolerant marine microalga using zeolite-based adsorption. Bioresour. Technol. 359, 127490.
22. Lourenço, S.O., Barbarino, E., Lavín, P.V., Lanfer Marquez, U.M., Aidar, E. 2004. Distribution of intracellular nitrogen in marine microalgae: calculation of new nitrogen-to-protein conversion factors. Eur. J. Phycol. 39:1, 17-32.
23. Lourenco, S. O., Barbarino, E., Mancini-Filho, J., Schinke, K. P., Aidar, E., 2002. Effects of different nitrogen sources on the growth and biochemical profile of 10 marine microalgae in batch culture: an evaluation for aquaculture. *Phycologia*, *41*(2), 158-168.
24. Martinez, K.A., Lauritano, C., Druka, D., Romano, G., Grohmann, T., Jaspars, M., Caridad, D., Cautain, B., Cruz, M. De, Ianora, A., Reyes, F., 2019. Amphidinol 22, a New Cytotoxic and Antifungal Amphidinol from the Dinoflagellate *Amphidinium carterae*. Mar. Drugs 17, 385.

25. Milani, D., Kiani, A., Haque, N., Giddey, S., Feron, P., 2022. Green pathways for urea synthesis: a review from Australia's perspective. Sustain. Chem. Climate Action 1, 100008.
26. Molina-Miras, A., López-Rosales, L., Cerón-García, M.C., Sánchez-Mirón, A., Olivera-Gálvez, A., García-Camacho, F., Molina-Grima, E., 2020a. Acclimation of the microalga *Amphidinium carterae* to different nitrogen sources: potential application in the treatment of marine aquaculture effluents. J. Appl. Phycol. 32, 1075-1094.
27. Molina-Miras, A., López-Rosales, L., Sánchez-Mirón, A., Cerón-García, M.C., Seoane-Parra, S., García-Camacho, F., Molina-Grima, E., 2018a. Long-term culture of the marine dinoflagellate microalga *Amphidinium carterae* in an indoor LED-lighted raceway photobioreactor: production of carotenoids and fatty acids. Bioresour. Technol. 265, 257–267.
28. Molina-Miras, A., López-Rosales, L., Sánchez-Mirón, A., López-Rodríguez, M., Cerón-García, M.C., García-Camacho, F., Molina-Grima, E., 2020b. Influence of culture medium recycling on the growth of a marine dinoflagellate microalga and bioactives production in a raceway photobioreactor. Algal Res. 47, 101820.
29. Morales-Amador, A., Molina-Miras, A., López-Rosales, L., Sánchez-Mirón, A., García-Camacho, F., Souto, M.L., Fernández, J.J., 2021. Isolation and structural elucidation of new amphidinol analogues from *Amphidinium carterae* cultivated in a pilot-scale photobioreactor. Mar. Drugs 19(8), 432.
30. Navarro López, E., Cerón García, M.C., López Rosales, L., Sánchez Mirón, A., García Camacho, F., Molina Grima, E., 2023. Phytosanitary formulation (Patent No. WO2022269118 (A1)). Spanish Patent and Trademark Office.
31. Park, Y. H., Han, S. I., Oh, B., Kim, H. S., Jeon, M. S., Kim, S., Choi, Y. E. , 2022. Microalgal secondary metabolite productions as a component of biorefinery: A review. Bioresour. Technol. *344*, 126206.
32. Remize, M., Planchon, F., Loh, A. N., Le Grand, F., Lambert, C., Bideau, A., ... & Soudant, P. (2020). Identification of polyunsaturated fatty acids synthesis pathways in the toxic dinophyte *Alexandrium minutum* using 13C-labelling. *Biomolecules* 10(10), 1428.

33. Ribeiro, D.M., Roncaratti, L.F., Possa, G.C., Garcia, L.C., Cançado, L.J., Williams, T.C.R., dos Santos Alves Figueiredo Brasil, B., 2020. A low-cost approach for *Chlorella sorokiniana* production through combined use of urea, ammonia and nitrate based fertilizers. Bioresour. Technol. Rep. 9, 100354.
34. Remize, M., Planchon, F., Loh, A.N., Le Grand, F., Bideau, A., Le Goic, N., Fleury, E., Miner, P., Corvaisier, R., Volety, A., Soudant, P., 2020. Study of synthesis pathways of the essential polyunsaturated fatty acid 20:5n-3 in the diatom *Chaetoceros muelleri* using ^{13}C-isotope labeling. Biomolecules 10, 797.
35. Renuka, N., Guldhe, A., Prasanna, R., Singh, P., Bux, F., 2018. Microalgae as multi-functional options in modern agriculture: current trends, prospects and challenges. Biotechnol. Adv. 36(4), 1255-1273.
36. Santin, A., Russo, M. T., Ferrante, M. I., Balzano, S., Orefice, I., Sardo, A., 2021. Highly valuable polyunsaturated fatty acids from microalgae: strategies to improve their yields and their potential exploitation in aquaculture. Molecules 26(24), 7697.
37. Seoane, M., Cid, Á., Esperanza, M., 2021. Toxicity of bisphenol A on marine microalgae: single- and multispecies bioassays based on equivalent initial cell biovolume. Sci. Total Environ., 767, 144363.
38. Solomon, C. M., Collier, J. L., Berg, G. M., Glibert, P. M., 2010. Role of urea in microbial metabolism in aquatic systems: a biochemical and molecular review. Aquat. Microb. Ecol. 59(1), 67-88.
39. Spiller, M., Moretti, M., De Paepe, J., Vlaeminck, S. E., 2022. Environmental and economic sustainability of the nitrogen recovery paradigm: Evidence from a structured literature review. Resour. Conserv. Recycl. 184, 106406.
40. Statista, 2022. Production capacity of urea worldwide from 2018 to 2030 (access date 06/07/23). https://www.statista.com/statistics/1063689/global-urea-production-capacity/
41. Su, Y., 2021. Revisiting carbon, nitrogen, and phosphorus metabolisms in microalgae for wastewater treatment. Sci. Total Environ. 762, 144590.

42. Su, Y., Jacobsen, C., 2021. Treatment of clean in place (CIP) wastewater using microalgae: Nutrient upcycling and value-added byproducts production. Sci. Total Environ. 785, 147337.
43. Thomas, Y., Thiebeauld, O., 2022. Use of an amphidinol for its fungicidal and/or bactericidal activity on fungi, oomycetes and/or pathogenic bacteria of plants and crop seeds (Patent No. US2022192194 (A1)). U.S. Patent and Trademark Office.
44. Urbańczyk, E., Sowa, M., Simka, W., 2016. Urea removal from aqueous solutions—a review. J. Appl. Electrochem. 46, 1011–1029.
45. Wellkamp, M., García-Camacho, F., Durán-Riveroll, L. M., Tebben, J., Tillmann, U., Krock, B., 2020. LC-MS/MS method development for the discovery and identification of amphidinols produced by *Amphidinium*. Mar. drugs, 18(10), 497.
46. Yaakob, M. A., Mohamed, R. M. S. R., Al-Gheethi, A., Aswathnarayana Gokare, R., Ambati, R. R., 2021. Influence of nitrogen and phosphorus on microalgal growth, biomass, lipid, and fatty acid production: an overview. *Cells*, *10*(2), 393.

Figure Captions

Figure 1. Dynamics of the sequential cultures of the microalga *Amphidinium carterae* in the bubble columns photobioreactors for the three nitrogen sources: nitrate (NIT), urea (URE), and ammonium (AMO). (**A**, **C**, **E**) Temporal changes in the biomass concentration (C_b, log scale), cells concentration (N, log scale), dissolved phosphate and nitrogen source concentrations in the supernatants; (**B**, **D**, **F**) cell fluorescence intensities relative to cell volume measured by the photomultiplier detectors *FL*1, *FL*2 and *FL*3 of the flow cytometer. S1: subculture 1; S2: subculture 2. Data points are averages and vertical bars are standard deviation.

Figure 2. Effect of nitrogen sources (NIT: nitrate; URE: urea; AMO: ammonium) on (**A**) maximum specific growth rate (μ_{max}), (**B**) maximum biomass productivity (P_{bmax}), (C) biomass-to-nitrogen yield ($Y_{b/N}$) and (D) biomass-to-phosphate yield ($Y_{b/P}$). Data points are the averages along with their standard deviation for duplicate cultures. Values denoted by a different lowercase at each point differ significantly at $p < 0.01$ in the one-way ANOVA.

824 **Figure 3**. (**A**) Heatmap of 43 ^{1}H NMR normalized bins from methanol:water (80:20 v/v) and
825 chloroform:methanol (80:20 v/v) extracts of *A. carterae* biomass containing specific assigned
826 metabolites for the 4 different experimental sets. The heatmap was built using Euclidean distances
827 and Ward clustering for metabolites showing statistically different contents between at least two
828 experimental sets. The color scheme represents the variation on metabolic content among the 4
829 experimental sets in a scale from light green (lowest content, -1.5) to light red (highest content,
830 1.5). Abbreviations: *ala* – alanine, *APD* – amphidinols class, *asp* – aspartate, *bet* – betaine, *chl a* –
831 chlorophyll a, *cho* – choline-based compounds, *DHA* - docosahexaenoic acid, *DMSP* –
832 dimethylsulfoniopropionate, *EPA* – eicosapentaenoic acid, *FA* – fatty acids, *form* – formate, *gal* –
833 galactose, *glc* – glucose, *gln* – glutamine, *glu* – glutamate, *ile* – isoleucine, *leu* – leucine, *lys* – lysine,
834 *n-3* – omega 3 FA, *phe* – phenylalanine, *pro* – proline, *PUFA* – polyunsaturated fatty acids, *pyr* –
835 pyruvate, *TAG* – triacylglycerols, *thr* – threonine, *trp* – tryptophan, *tyr* – tyrosine, *UFA* –
836 unsaturated fatty acids, *urid* – uridine, *val* – valine. (**B**) Volcano diagram of the differential
837 metabolites displaying in ordinate the level of significant difference (– log10(*p*-value)). The
838 abscissa displays the expression fold change (log_2FC). VIP was set above > 1. Vertical lines
839 represent threshold log_2FC values of ±0.263 for significant changes above 20% (i.e. FC>1.2 and
840 FC<0.83). (See Abbreviations in Figure 3A legend). (**C**) Enrichment pathways of URE-S2 *vs* NIT-
841 S2 presented in bubble chart. Each bubble represents a metabolic pathway. The X-axis of the
842 bubble and the bubble scale indicate the influence factor of the pathway in the topology analysis.
843 The larger the size, the greater the influence factor; the Y-axis and the colour of the bubble
844 indicate the enrichment analysis. P value (take the negative natural logarithm, namely –log10(p),
845 the redder the colour, the smaller the P value, the more significant the enrichment degree.
846 **Figure 4.** (**A**) PLS score contributions and (**B**) loadings plots obtained from ^{1}H NMR normalized
847 bins from methanol:water (80:20 v/v) and chloroform:methanol (80:20 v/v) extracts of *A.*
848 *carterae* biomass. The APD containing bin at δ_H 4.99 ppm was selected as Y variable. (**C**) List of
849 the metabolites that contribute most to the discrimination of the PLS model through the analysis
850 of their VIP values. Blue and red colored metabolites showed VIP values > 1, meaning that were
851 found to be positively (in blue) and negatively (in red) correlated with APD increase. (**D**) Activity

852 of methanolic extracts against agriculture phytopathogens measured as percentage of growth
853 inhibition relative to control. Extracts were prepared from dry *Amphidinium carterae* biomass
854 harvested in nitrate and urea grown PBR (NIT-S2 and URE-S2, respectively). Data points are
855 averages for duplicate samples. Data points are the averages along with their standard deviation
856 for duplicate samples.

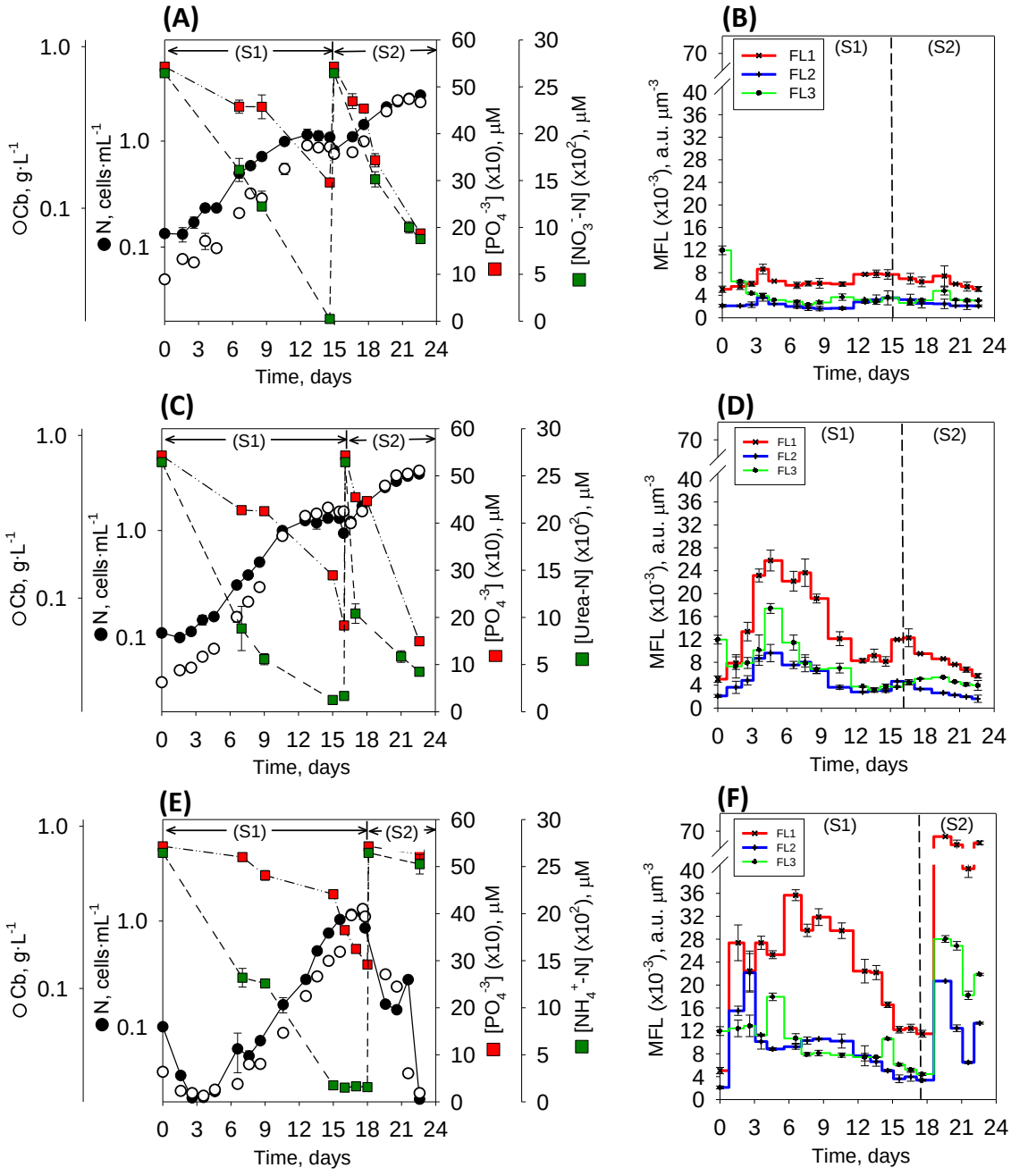

Figure 1

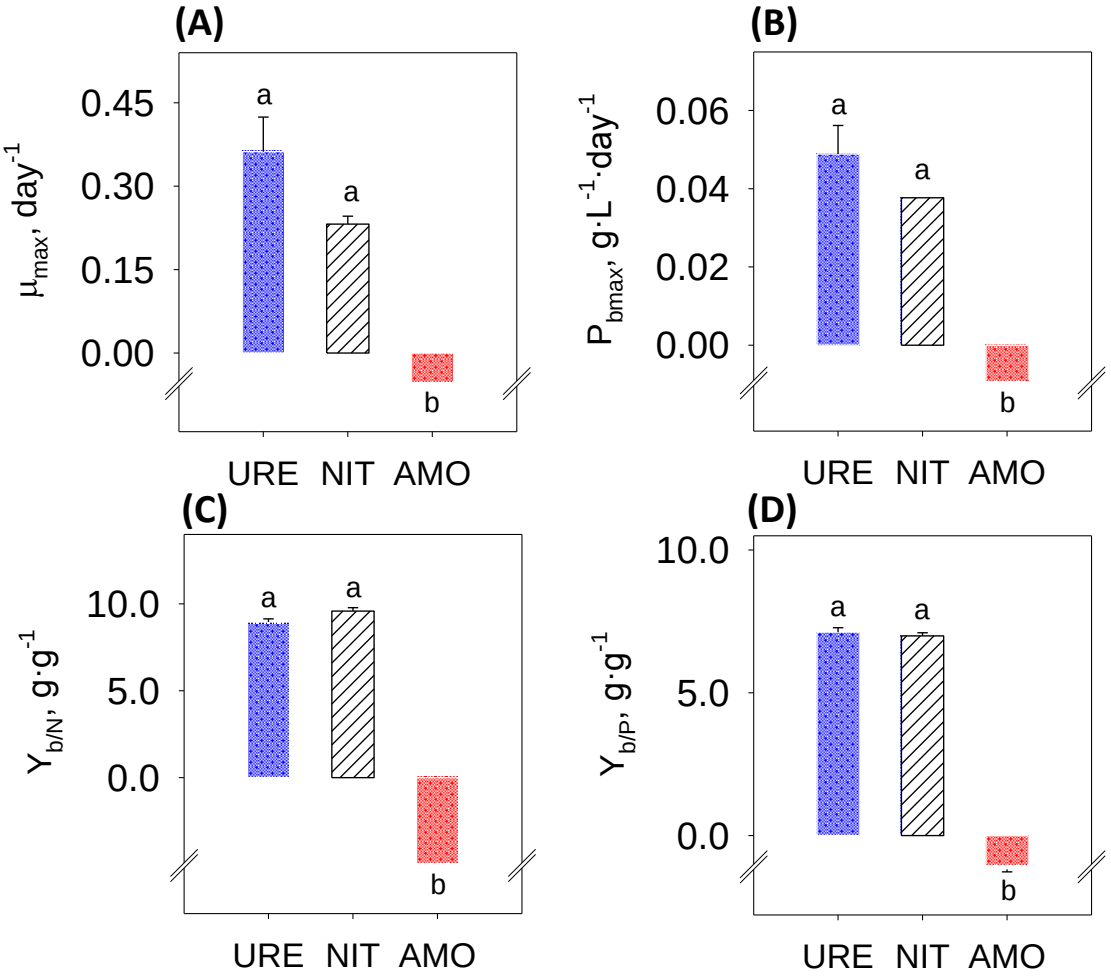

Figure 2

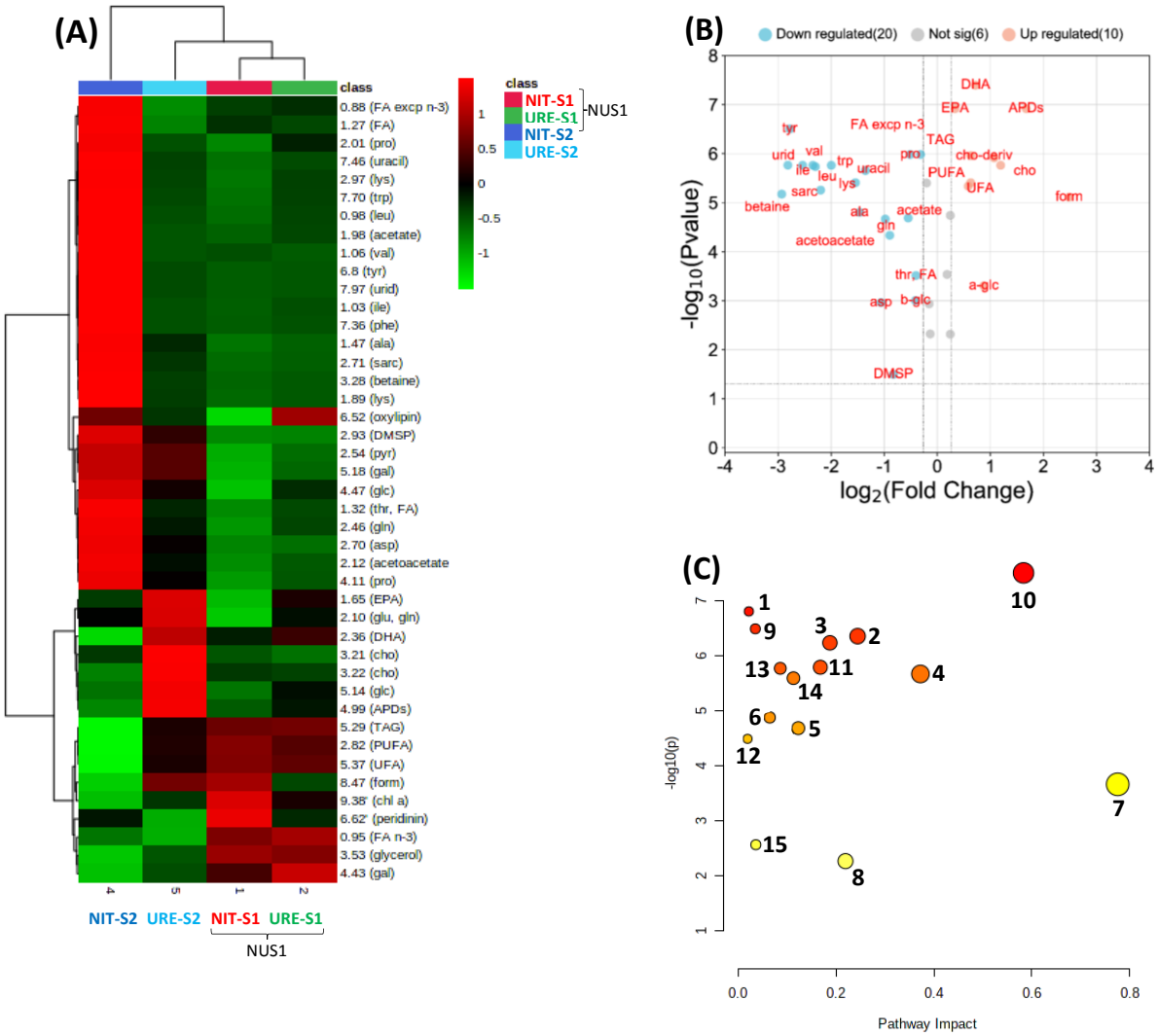

Figure 3

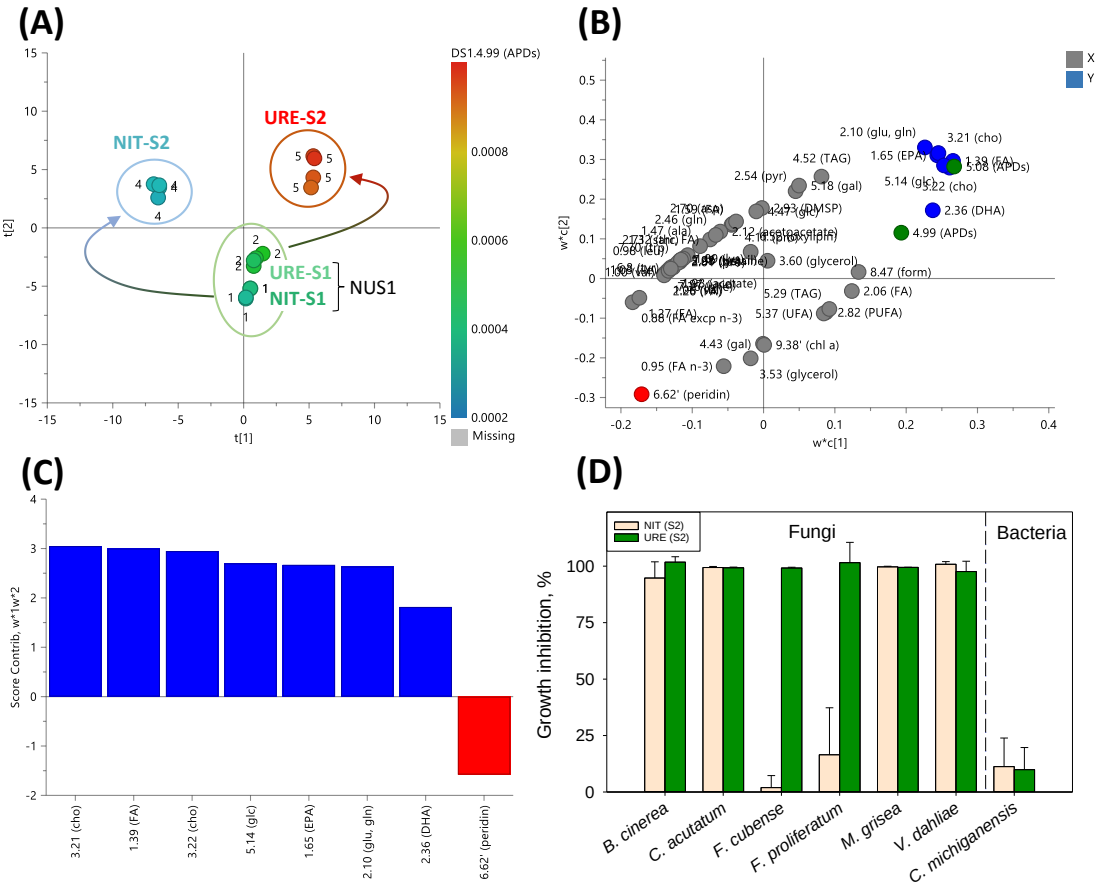

Figure 4

Accepted manuscript. https://doi.org/10.1016/j.biortech.2023.129643

CRediT author statement

A. Molina-Miras: Conceptualization, Data curation; Formal analysis; Investigation; Methodology; Writing – original draft; Writing - review & editing. **A.C. Abreu:** Investigation, Formal analysis, Validation, Writing - review & editing. **L. López Rosales:** Conceptualization; Methodology. **M.C. Cerón-García:** Conceptualization; Funding acquisition; review & editing. **A. Sánchez-Mirón:** Conceptualization; Funding acquisition; Project administration; review & editing. **I. Fernández:** Funding acquisition, Supervision, Validation, Writing - review & editing. **F. García-Camacho:** Conceptualization, Methodology, Formal analysis, Visualization, Supervision, Writing - Original Draft, Review & Editing, Project administration, Funding acquisition.

Accepted manuscript. https://doi.org/10.1016/j.biortech.2023.129643